Dynamic and Steady-State Analysis of an Auto-Regulator in a Flow Divider and/or Combiner Valve

M. Fedoroff
Graduate Student (U of S) and Engineer,
Northern Telecom Canada Limited,

R. T. Burton

G. J. Schoenau

Department of Mechanical Engineering,
University of Saskatchewan,
Saskatchewan, Canada

Y. Zhang
Department of Mechanical Engineering,
Wuhan Institute of Technology,
Wuhan, People's Republic of China

Flow divider and/or combiner valves are hydraulic components which are used to divide and/or combine flow in a predetermined ratio independent of loading conditions. Over the past years the authors have successfully designed valves which can divide and/or combine flow with an error of less than 3 percent for all loading conditions. More recently, a valve which can be used to divide and combine flow for a wide range of flow requirements and still maintain an error of less than 3 percent has been developed and has been labeled an "auto-regulated high precision flow divider/combiner valve". The heart of the auto-regulated valve is the auto-regulator itself. In this paper, the operation of the regulator is discussed and design criterion for acceptable performance presented. A linearized model is developed from which a number of valve parameters are established. A more complex model using the Power Bond Graph technique is presented, and transient responses to different flow inputs are compared to experimental data. The model and experimental responses were in good agreement; hence, it was concluded that the model could be used with confidence in future stability studies.

Introduction

Synchronous valves, (henceforth referred to as flow divider and/or combiner valves, shortened to flow divider/combiner valves for convenience), are used in circuits in which synchronized movement of two actuators or motors are required or indeed, when two independent flow sources and/or sinks are required. As an example, lifting hydraulically the two "wings" of a cultivator requires synchronous motion of the two driving actuators. Flow divider/combiner valves are used to regulate the flow to or from each actuator at a prescribed ratio.

Most commercial valves are capable of dividing or combining flow with an accuracy of 90 to 97 percent (Tauger, 1972; Kwan et al., 1979). (In the literature, flow dividing/combining error is used rather than flow accuracy; hence, flow error will be adopted in this paper.) In many applications, an error of 3 percent or greater is not acceptable. For example, in the cultivator example quoted above, if the division of flow is not equal, an imbalance in the wings weight distribution could result in the cultivator tipping over. Studies oriented towards understanding the source of flow error and methods of compensating for them, have been initiated by the authors and others (Kwan et al., 1979; Burton et al., 1980; Chan et al., 1981; Zhang et al., 1984; Zhang et al., 1985).

In 1979, Kwan developed a two stage flow divider valve which was capable of dividing flow with an error of less than 1.5 percent for large pressure differentials across the load ports. Chan (1981) designed a single stage flow divider valve which was of the same complexity as existing valves but was able to divide flow within 2 percent for all loads considered. In 1984, Zhang applied Chan's basic design concept to a flow divider and combiner valve by using a combination of shuttle valves and dual piston arrangement. This valve was able to divide and combine flow within 2 percent for large pressure differentials across the load.

The high precision valves noted above were designed to control about a fixed operating flow point. If the flow requirements were changed, the flow dividing/combining error also changed (sometimes reducing the error and other times making it worse). To address this problem, Zhang (1986, 1988) designed an "auto-regulator" which would compensate for changes in the flow through the combiner/divider valve. Initial studies found that the auto-regulator could maintain a flow error of less than 2 percent which was relatively independent of changes in both load pressure and flow. This valve was found initially to show some instability in the combining mode and was subsequently analyzed by Zhang and Xin (1989). This study was limited in its scope but the authors reported good agreement between simulated and experimental test responses. Existence of instabilities reported in earlier work was not verified in this study.

The auto-regulator is the "heart" of Zhang's combiner/divider valve. It is this device which allows the extension of

Contributed by the Dynamic Systems and Control Division for publication in the JOURNAL OF DYNAMIC SYSTEMS, MEASUREMENT, AND CONTROL. Manuscript received by the Dynamic Systems and Control Division January 15, 1991; revised manuscript received June 20, 1991. Associate Editor: A. Akers.

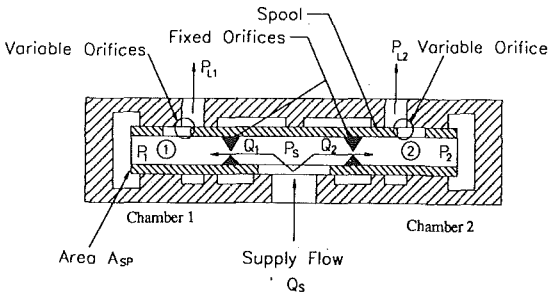

Fig. 1 Configuration of a standard flow divider valve

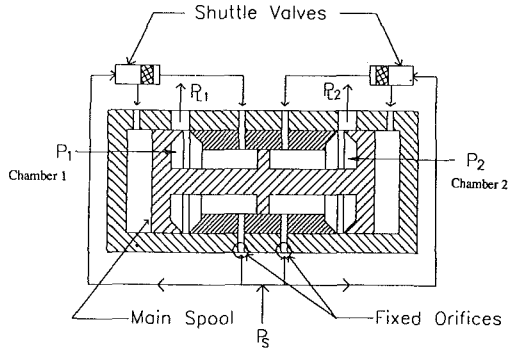

Fig. 2 High precision flow divider/combiner valve

the flow range of the combiner and/or divider valve. Earlier studies of combiner/divider valves have been reported, but the operation of the auto-regulator has not been considered in any depth. Because its performance statically and dynamically are so critical to the overall performance of the combiner/divider valve, a complete experimental and analytical study of the auto-regulator by itself was initiated. The auto-regulator was redesigned to accommodate the measurement of critical parameters. The system was analyzed mathematically; steady state and dynamic transient responses were obtained from the simulated model and compared to experimental data. This paper, then, will present the results of this analytical and experimental study of the auto-regulator valve.

Operation of the Flow Divider/Combiner Valve

In order to understand how an auto-regulator operates, it is important to describe the mechanics of flow division and flow combination. Since the basic concept for both dividing and combining modes is similar, only the operation of a very simple flow divider valve is considered. Figure 1 is a cross-section of a typical flow dividing valve. If pressures P_1 and P_2 are not equal due to unequal load pressures, P_{L1} and P_{L2}, then the spool is forced to move. As a result, the area of the variable orifices are adjusted (and thus the pressure loss across them) until P_1 and P_2 are equal. Practically, the presence of flow reaction forces on the spool means that P_1 and P_2 can never be exactly equal and hence some flow dividing error will exist. (It should be noted that a great deal of research on improving the accuracy of these valves has revolved around reducing the magnitude of these types of forces.)

The flow rate through the fixed orifices is represented mathematically by:

$$Q_1 = C_d A_{f1}\sqrt{2(P_S - P_1)/\rho} \tag{1}$$

$$Q_2 = C_d A_{f2}\sqrt{2(P_S - P_2)/\rho} \tag{2}$$

If flow is to be divided equally, as is usually the case, then $A_{f1} = A_{f2}$.

The steady-state flow dividing error can be expressed as (Kwon, 1979):

$$\%E = \frac{\Sigma F_i}{(2A_{Sp}\Delta P_f)} * 100 \tag{3}$$

It is apparent from Eq. (3), that if the pressure drop across the fixed orifices is too low, the flow dividing error increases. However, a valve with a large pressure drop is not energy efficient. It is possible to use an auto-regulator to effectively provide a variable orifice resulting in a relatively low pressure drop at high flow rates. This produces a valve which is accurate and energy efficient over a wide operating range.

Figure 2 is a schematic representation of a high precision flow divider/combiner valve. For the dividing mode, flow enters through the fixed orifices at supply pressure, P_S. The supply pressure is connected to one side of the shuttle valves while the pressures, P_1 and P_2, are connected to the other side. This forces the spools to the position shown in Fig. 2. With the shuttle valves in this position, the supply pressure is connected to the outside area of the main spool. Operation is the same as the flow divider valve discussed previously.

In the combiner mode, the supply pressure becomes the downstream (or tank) pressure. Flow enters chambers 1 and 2 through the variable orifices. Since the pressure in chambers 1 and 2 are greater than the downstream pressure, the shuttle

Nomenclature

A_{f1} = area of fixed orifice 1, m^2
A_{f2} = area of fixed orifice 2, m^2
A_{P1} = cross-sectional area of piston 1, m^2
A_{P2} = cross-sectional area of piston 2, m^2
A_r = cross-sectional area of piston 2 rod, m^2
A_{SP} = cross-sectional area of HPSV spool, m^2
A_{V1} = area of the variable orifice 1, m^2
A_{V2} = area of the variable orifice 2, m^2
b_1 = coefficient of viscous friction (piston 1), Ns/m
C_1 = capacitance of chamber 1, m^3/Pa
C_2 = capacitance of chamber 2, m^3/Pa
C_d = coefficient of discharge
C_r = clearance between piston and sleeve, m
D = diameter of piston, m
D_{P1} = diameter of piston 1, m
D_{P2} = diameter of piston 2, m
E = modulus of elasticity for steel, Pa
F_f = viscous friction force, N
F_i = resultant force on HPSV spool, N
F_{m1} = resultant force on piston 1, N
F_{m2} = resultant force on piston 2, N
F_O = pretension in spring, N
I_1 = inertia of piston 1, $Nmsec^2$
I_2 = inertia of piston 2, $Nmsec^2$
k_e = effective spring constant acting on spools, N/m
K_i = spring coefficient of piston 2 rod, N/m
K_S = force displacement constant of the spring, N/m
K_{ST} = spring constant of piston stop, N/m
L = length of damping orifice, m
L_P = length of the piston, m
L_r = length of piston 2 rod, m
m_1 = mass of piston 1, kg
P_1 = HPSV chamber 1 pressure, Pa
P_2 = HPSV chamber 2 pressure, Pa
P_{C1} = pressure in chamber 1, Pa
P_{C2} = pressure in chamber 2, Pa
P_E = entrance/exit pressure loss, Pa
ΔP_f = pressure loss across fixed orifices, Pa
P_{L1} = HPSV load pressure 1, Pa
P_{L2} = HPSV load pressure 2, Pa
P_S = supply pressure, Pa
P_{SC} = pressure in supply chamber, Pa

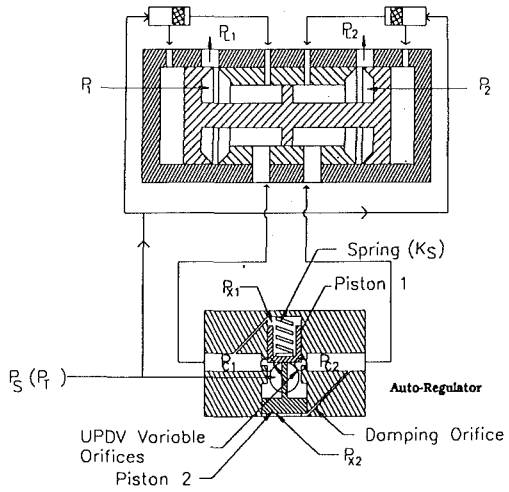

Fig. 3 High precision flow divider/combiner valve with auto-regulator

valves are forced to move to the opposite position, connecting pressures P_1 and P_2 to the outside area of the main spool, providing the pressure compensation necessary to minimize flow combining error.

Concept of Auto-Regulation

In the auto-regulator design, the fixed orifices are replaced by variable orifices having a pressure drop independent of flow. Figure 3 is a sketch of the cross section of the auto-regulator as designed by Zhang et al. (1986), showing the porting between the auto-regulator and flow divider/combiner valve.

To aid in understanding how the auto-regulator works, an example of its operation in the dividing mode is considered. With reference to Fig. 3, flow enters the auto-regulator at supply pressure P_S and exits through the variable orifices with the two streams entering the divider/combiner valve at ports A and B. The pressure downstream of one of the auto-regulator variable orifices is connected through a damping orifice to the spring side of the auto-regulator piston. Due to the pressure loss across this variable orifice, the pressure on the spring side of the piston is less than the supply pressure. The auto-regulator is designed so that, at rest, the spring is compressed and the piston will not move until the difference in pressure across it is large enough to overcome the initial compression force of the spring. As the flow rate through the auto-regulator increases, the pressure difference across the piston also increases causing the piston to move. This results in further compression in the spring and an increase in the area of the variable orifices. The piston continues to adjust the area of the variable orifices until the pressure and spring forces are in balance.

If the initial compression force of the spring is large compared with the added spring force caused by the additional compression, then the pressure loss across the auto-regulator variable orifices remains approximately constant. Thus, changes in flow result in similar changes in the variable orifice area while maintaining an approximately constant pressure loss and therefore expanding the flow range without increasing pressure loss.

The equations describing the steady state motion of the auto-regulator divider/combiner valve provide additional insight into performance characteristics. In the dividing mode, a force balance on piston 1 for the auto-regulator shown in Fig. 3 yields

$$0 = P_S A_{P1} - P_{X1} A_{P1} - K_S(x_{S0} + x_1) \tag{4}$$

Note that piston 2 will be forced against the bottom stop because the supply pressure is greater than the pressure downstream of the variable orifice, P_{C2}.

For steady state conditions, the pressure on the top side of the piston, P_{X1}, is equal to the pressure in chamber 1, P_{C1}, and Eq. (4) can be written as

$$P_S - P_{C1} = K_S(x_{S0} + x_1)/A_{P1} \tag{5}$$

If x_{S0}, the initial compression length of the spring, is much greater than x_1, the displacement of piston 1, then the pressure drop across the variable orifices will remain relatively constant.

In the combining mode, flow is reversed through the valve. The pressure upstream of one of the variable orifices is connected to the bottom side of piston 2. The supply pressure becomes the downstream or tank pressure which is less than P_{C2} and piston 2 is now forced up in contact with piston 1. For steady-state conditions, pistons 1 and 2 can be analyzed a single unit. The force balance on this piston combination becomes

$$0 = P_T(A_{P1} - A_r) - P_T(A_{P2} - A_r) + P_{X2}A_{P2} - P_{X1}A_{P1} - K_s(x_{S0} + x_1) \tag{6}$$

Under steady state conditions, $P_{C1} = P_{C2}$ and therefore $P_{X1} = P_{X2}$ which simplifies Eq. (6) to

$$(P_{C1} - P_T)A_{P2} - (P_{C1} - P_T)A_{P1} = K_S(x_{S0} + x_1) \tag{7}$$

Nomenclature (cont.)

P_{SC1} = pressure loss across variable orifice 1, Pa
P_T = pressure downstream from the load, Pa
P_{X1} = pressure on spring side of piston 1, Pa
P_{X2} = pressure on spring side of piston 2, Pa
Q_1 = flow rate exiting chamber 1, m^3/s
Q_2 = flow rate exiting chamber 2, m^3/s
Q_C = flow rate due to capacitance effects, m^3/s
Q_{C1} = flow rate through variable orifice 1, m^3/s
Q_{C2} = flow rate through variable orifice 2, m^3/s
Q_{D1} = flow rate through damping orifice 1, m^3/s
Q_{D2} = flow rate through damping orifice 2, m^3/s
Q_E = exit flow rate, m^3/s
Q_{P1} = leakage flow past piston 1, m^3/s
Q_{P2} = leakage flow past piston 2, m^3/s
Q_{X1} = flow resulting from velocity of piston 1, m^3/s
Q_{X2} = flow resulting from velocity of piston 2, m^3/s
Q_S = supply flow, m^3/s
Q_{SC} = capacitance flow in supply line, m^3/s
r = radius of damping orifice 1, m
s = Laplace operator
R_{D1} = impedance of damping orifice 1, Pa s/m^3
R_{T1} = impedance of chamber 1, Pa s/m^3
w = area gradient of variable orifice, m^2/m
x_{S0} = precompressed length of the spring, m
x_0 = minimum open length of variable orifices, m
x_1 = displacement of piston 1, m
$\dot{x}_1$ = velocity of piston 1, m/s
$\ddot{x}_1$ = acceleration of piston 1, m/s^2
x_2 = displacement of piston 2, m
$\dot{x}_2$ = velocity of piston 2, m/s
$\ddot{x}_2$ = acceleration of piston 2, m/s^2
ρ = density of the fluid, kg/m^3
μ = viscosity of the oil, N s/m
π = pi
ζ_v = UPDV damping ratio
ω = natural frequency, rad/s

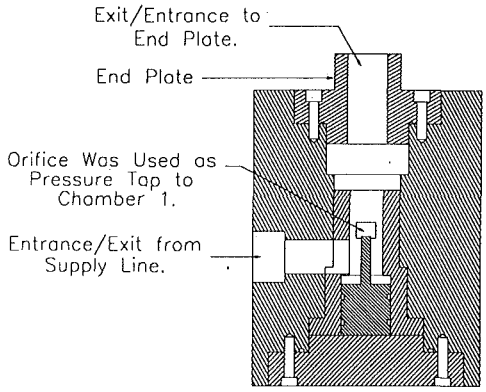

Fig. 4 Auto-regulator with special transducer adapters for particular experimental tests

If $A_{P2} = 2A_{P1}$, then Eq. (7) reduces to Eq. (5) and the pressure drop will theoretically react in a manner identical to that of the dividing mode.

Steady-State Performance

The experimental test valve appropriately modified to accommodate transducers for the static and dynamic experimental studies is illustrated in Fig. 4. A complete analysis and design of the auto-regulator based on specified steady state performance criteria has been presented in a previous paper (Fedoroff et al., 1990) and will not be repeated here. However, the measured and predicted pressure drop across the variable orifice in both combining/dividing modes of the auto-regulator is worth repeating here. The regulated pressure drop as a function of flow rate is shown in Figs. 5 and 6 for the dividing and combining modes respectively.

There are two types of pressure losses to consider. The first is the loss due to the size and shape of the valve passageway without the pistons present. It is most desirable to minimize this type of a loss since it cannot be controlled by the auto-regulator. The second pressure loss is that across the variable orifices and as such, is regulated by the pistons. In Figs. 5 and 6, the variable pressure loss was calculated by subtracting the losses of the first type from the combined pressure losses when the pistons were physically present in the valve.

In the dividing mode, the agreement with theory is very good. However, in the combining mode, a noticeable difference was observed. An attempt was made to identify the source of the error. At the time of the writing of this report, a satisfactory explanation could not be forwarded and thus remains an area of future specialized study. In the dynamic studies this discrepancy was translated into an "equivalent reaction force" and hence was subsequently included in all appropriate describing equations.

In summary, the relatively constant pressure drop as a function of flow rate indicated that the auto-regulator did indeed regulate pressure with varying flow rates as required.

Dynamic Analysis of the Auto-Regulator

A design consideration which could not be deduced from the steady state describing equations but which was of utmost importance from a dynamic point of view, was the size of damping orifices in various feedback paths (Fig. 3). To investigate orifice sizing, a linearized analysis of the auto-regulator was carried out based on the following assumptions:

1. Flows through controlling orifices were turbulent.
2. Flows through damping orifices were laminar.
3. Fluid capacitance at the top of piston 1 and below piston 2 as well as the entrance were negligible compared to the actual chambers 1 and 2.
4. Leakage past the pistons was negligible.

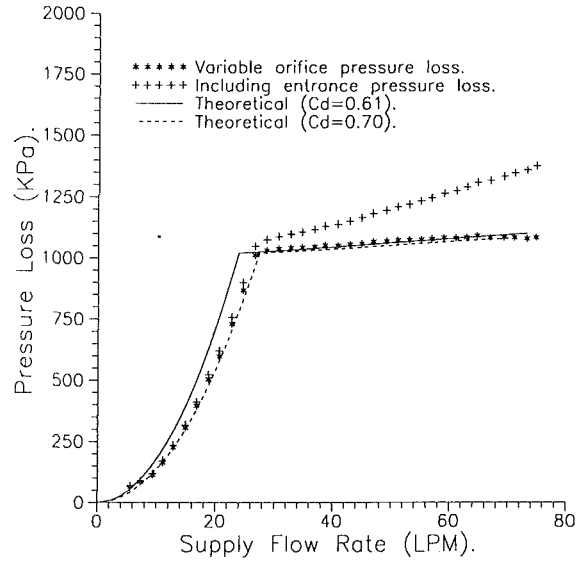

Fig. 5 Pressure drop across variable orifice as a function of supply flow rate: divider mode

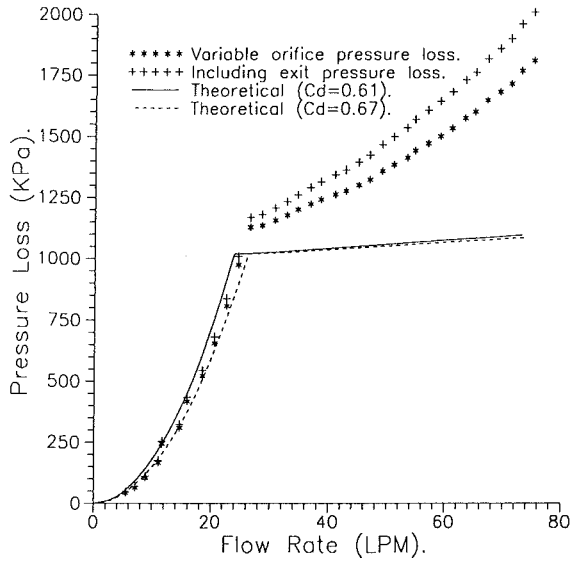

Fig. 6 Pressure drop across variable orifice as a function of supply flow rate: combiner mode

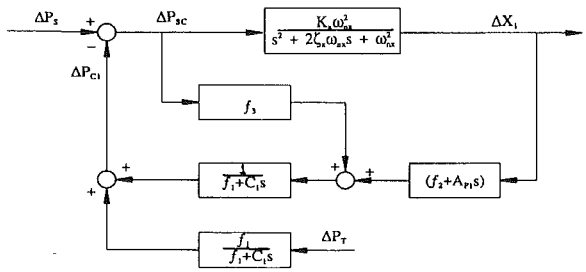

Fig. 7 Block diagram of linearized model

5. Chamber pressures P_{C1} and P_{C2} were equal.
6. Friction forces on the spool were viscous.
7. Variations in all variables are small (necessary for small signal analysis).

The describing equations for the auto-regulator in their linearized form are listed in Appendix A. The transfer function relating the pressure drop across the variable orifice to changes in the supply pressure is given by Eq. (8) and is shown in block diagram form in Fig. 7.

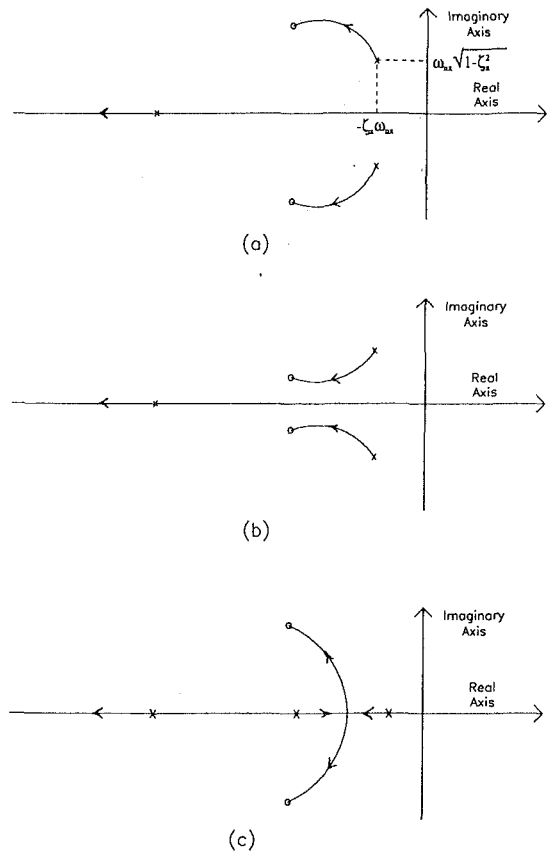

Fig. 8 Poles and zeros possibilities for linearized model

Table 1 Final dimensions and parameter limits of the auto-regulator

Parameters	*Design Dimensions*	*"As-built" Dimensions*[4]
x_0	0.60 mm	0.68 mm
x_{s0}	16.00 mm	16.10 mm
Maximum x_1	1.40 mm	1.40 mm
D_{P1}	10.00 mm	9.98 mm
D_{P2}	14.10 mm	14.10 mm
K_s	4640 N/m[1]	4949 N/m[2]
Minimum Q_s	20.5 LPM	23.9 LPM[5]
Maximum Q_s	71.4 LPM	75.7 LPM[5]
Minimum ΔP_{sc}	945 KPa	1017 KPa[5]
Maximum ΔP_{sc}	1028 KPa	1105 KPa[5]

[1] Manufacturers specification [12].
[2] Determined experimentally.
[3] Increase in variable orifice pressure loss of 8.7%.
[4] Linear measurement accuracy is ± 0.02mm.
[5] Calculated using as-built dimensions.

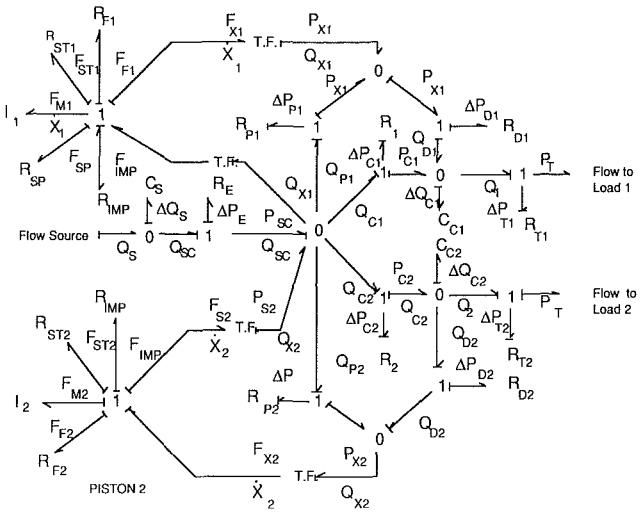

Fig. 9 Bondgraph of auto-regulator

$$\frac{\Delta P_{SC1}}{\Delta P_S} = \frac{1}{1+\dfrac{f^3/C1\{s^2+[2\zeta_x\omega_{nx}+(A_{P1}K_x\omega_{nx}^2/f_3)]s+\omega_{nx}^2+K_x\omega_{nx}^2(f^2/f_3\}}{(f^1/C1+s)(s^2+2\zeta_x\omega_{nx}S+\omega_{nx}^2)}} \tag{8}$$

The development of this transfer function is given in Appendix B. With respect to this transfer function, since C_1 is very small, it can be shown that

$$f_1/C_1 >> \zeta_x\omega_{nx}, \tag{9}$$

$$f_1/C_1 > \frac{[2\zeta_x\omega_{nx}+(A_{P1}K_x\omega_{nx}^2/f_3)]}{2}, \tag{10}$$

Assuming that the open loop zeros are complex, then

$$[2\zeta_x\omega_{nx}+(A_{P1}K_x\omega_{nx}^2/f_3)]^2 < 4[\omega_{nx}^2+K_x\omega_{nx}^2(f^2/f_3)]. \tag{11}$$

ζ_x was designed to be less than one. Therefore, two of the poles are complex conjugates. Three possible positions of the poles and zeros of the open loop equation are shown in Fig. 8, for the parameters used in the auto-regulator design. It can be seen that the complex poles dominate; hence, an estimate of the valve damping can be made from the expression

$$\zeta_v = \zeta_x = \frac{b_1 + A_{P1}^2 R_{D1}}{2\sqrt{m_1 f_4}}. \tag{12}$$

Since the only parameter whose dimension could be controlled was the damping orifice impedance, the sizing of the orifice was dictated by a calculation of R_{D1} as given by (Blackburn et al., 1967):

$$R_{D1} = \frac{8\pi L}{\mu r^4}. \tag{13}$$

A decision as to the appropriate orifice diameter dimension was made so as to satisfy Eq. (11) for a damping ratio of approximately .71 to achieve a stable but rapid response.

The linearized analysis played an integral part in designing the auto-regulator in its present form and gave a good indication of how the component should respond in a dynamic sense. A summary of all parameter values and component dimensions used in the final design is given in Table 1.

Bond Graph Model of the Auto-Regulator

The linearized model of the regulator was sufficient to provide a general idea of what the dynamic response of the regulator might be to small time-varying changes in the load pressure or supply flow, etc. However, since many of the describing equations of the auto-regulator are non-linear, the small signal analysis is no longer an adequate tool when the number of nonlinearities of the model are numerous or changes in any of the operating conditions are substantial. It was necessary, therefore, to use other techniques to solve the complex set of describing equations.

To facilitate the modelling process, the Power Bond Graph technique was used (Barnard and Dransfield, 1977 and Thoma, 1990). This technique graphically models the flow of power through hydraulic components and greatly facilitates the development of the describing equations and the assigning of proper causality of various relationships. A detailed description of this technique is not within the scope of this paper and the interested reader is directed to the reference quoted.

Two Bond graphs were developed for the auto-regulator

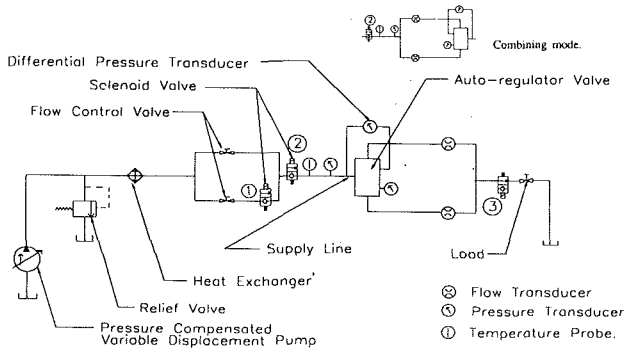

Fig. 10 Test stand for dynamic response tests

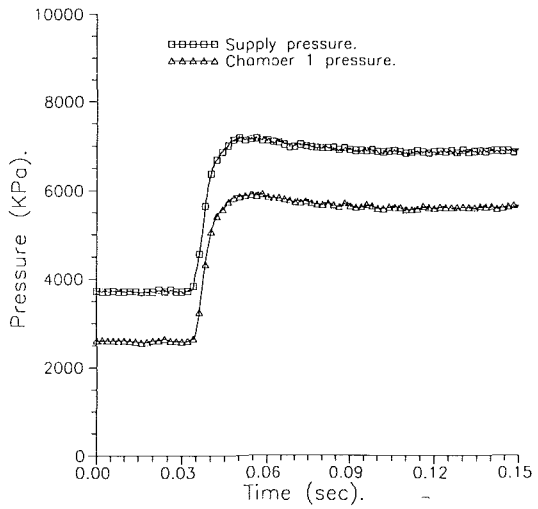

Fig. 11 Flow through variable orifices: dividing mode

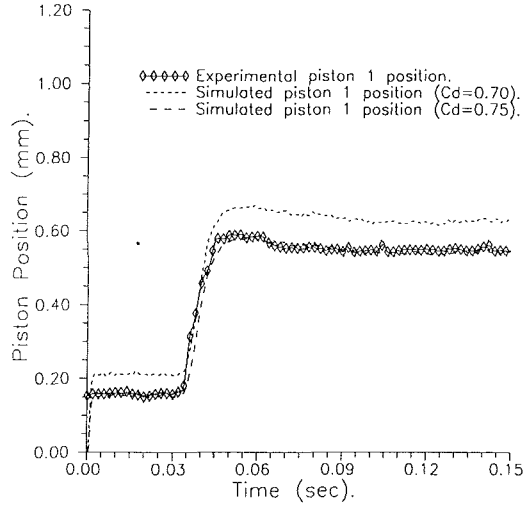

Fig. 12 Response of piston to a step change in flow rate: dividing mode

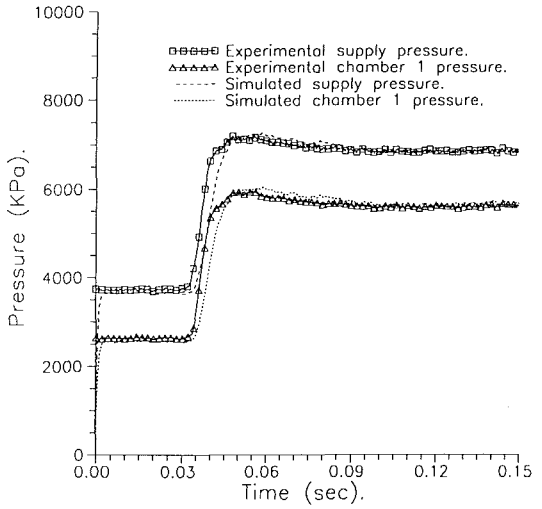

Fig. 13 Supply and chamber pressure response to a step change in flow rate: dividing mode

reflecting the two modes of operation. For brevity purposes, only the divider Bond graph is shown in Fig. 9. The combiner Bond graph is similar and can be found in Fedoroff (1990). Special consideration had to be made in the modelling of the pistons. This was because in the dividing mode, the pistons were separated. However, in the combining mode, pistons 1 and 2 acted as two masses separated by a stiff spring. The spring constant was determined using Hooks law as applied to the rod portion of piston 2. It should also be noted that the "equivalent reaction force" discussed earlier was also included in the model.

The assumptions used in the linearized model (excluding the small variation of parameters) were again used with a few more added to reflect the complete auto-regulator system. These additional assumptions were (reference Fig. 3):

(1) Flow forces on piston 1 were negligible

(2) The spring force was linear with piston 1 displacement

(3) The effect of the change in the cross-sectional area of piston 1 due to contact with the rod of piston 2 was negligible

(4) The capacitance of the supply chamber and chambers above and below the pistons are lumped with the supply/tank and chambers 1 and 2 respectively.

Based on the Bond graph of Fig. 9, the describing equations were developed and are listed in Appendix C. It is readily apparent that the describing equations are highly nonlinear. To solve these equations, a commercial package called TUTSIM was used. This particular package was used because nonlinear relationships could be modelled mathematically or with experimental data in the form of look-up tables. In the simulation, the "passage" (or entrance/exit) pressure losses and the pressure drops across the damping orifices were expressed as look-up tables. An additional advantage of TUTSIM was that it accommodated the Power Bond Graph representation directly.

Experimental Verification of Auto-Regulator Model

The circuit used to determine the dynamic response of the regulator to various inputs is illustrated in Fig. 10 for the dividing and combining modes respectively. The test stand was designed such that the effects of "step" changes in flow rate and downstream pressure on appropriate parameters such as piston position, etc. could be observed and recorded. For each test, the actual input parameter waveform was recorded and used as the input to the simulation (via a look-up table). This was deemed necessary because a true "step" in flow or pressure was not physically possible to create experimentally. The outputs were recorded using appropriate instrumentation and data collection devices.

Many experimental and theoretical transient responses were recorded and analyzed. Only a few representative waveforms will be presented. In the first case, the flow to the regulator in the divider mode was changed as indicated in Fig. 11. (In fact, Fig. 11 shows the flow through the individual orifices. The total flow is the sum of the two.) The total flow waveform was digitized and subsequently became the input to the simulation. The corresponding transient response of the piston position and supply and chamber pressure (theoretical and experimental) are shown in Figs. 12 and 13. For the combining

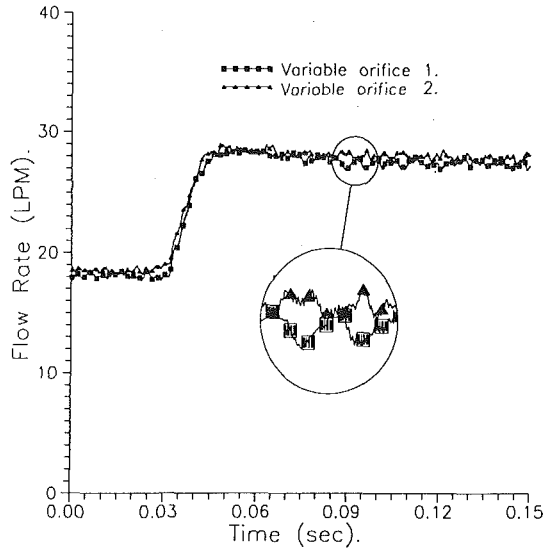

Fig. 14 Flow through variable orifices: combining mode

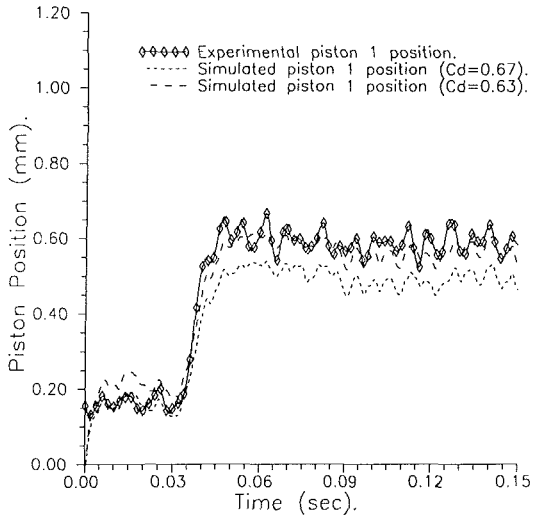

Fig. 15 Response of piston to a step change in flow rate: combining mode

mode and for a flow input illustrated in Fig. 14, the simulated and experimental piston position and supply pressure transients are shown in Figs. 15 and 16.

Agreement between the predicted and measured responses was very good for the pressure traces. However, a somewhat systematic error was noted in the simulated position of the piston 1. Small errors in assigning the discharge coefficients of the variable orifices have a significant effect on the piston simulated results as indicated in Figs. 12 and 15. Difficulties in accurately and reliably measuring the discharge coefficients precluded the authors from substantiating that indeed, physically, the discharge coefficients assumed these values. The authors believe however, that the basic dynamic waveforms of the theoretical and measured piston displacement are in excellent agreement.

Discussion and Conclusions

As evident in the transient response figures, the combiner mode showed a greater tendency to oscillate than in the divider mode. This, in part, was due to the oscillatory nature of the input flow sources in the combiner tests. This implies that the assumption of pure flow inputs was, in fact, only partially correct. Some interactions between the input flow and the auto-

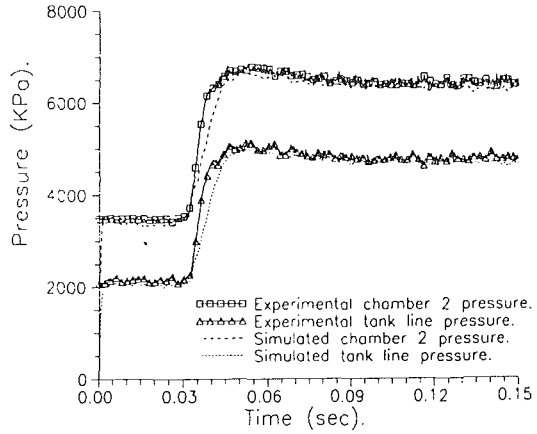

Fig. 16 Supply and chamber pressure response to a step change in flow rate: combining mode

regulator did exist and although this was partially reflected in the transient responses by using actual flow waveforms as the inputs, the model could not be used to isolate the source of the interaction. It would appear that the only way to account for this situation would be to model the complete testing system; this was considered to be beyond the scope of this study at present since the aim was to specifically examine the performance of the auto-regulator by itself. It is a study, however, that should be attempted to get a feeling for how component interactions occur in a much broader sense.

Specifically, with regard to the study on the auto-regulator, the following conclusions were drawn:

(1) The auto-regulator valve as designed could regulate the pressure drop across the variable orifices and hence provide a means of extending the range of a flow divider/combiner valve.

(2) The linearized analysis of the auto-regulator provided an effective design tool for such things as the sizing of damping orifices and showing the sensitivity of various parameters on the response of the regulator.

(3) The Bond Graph Model of the auto-regulator showed excellent agreement between the predicted and measured transient responses. The model could not be used with confidence in a comprehensive model of the auto-regulator and the combiner/divider valve.

Acknowledgments

The authors gratefully acknowledge the provisions of funds for this work from the Natural Sciences and Engineering Research Council of Canada.

References

Barnard, B., and Dransfield, P., 1977, "Predicting Responses of a Proposed Hydraulic Control System Using Bond Graphs," Trans. ASME, JOURNAL OF DYNAMIC SYSTEMS, MEASUREMENT AND CONTROL, Vol. 99.

Blackburn, J. F., Reethof, G., and Shearer, J. L., 1967, *Fluid Power Control*, The M.I.T. Press, Cambridge, Mass.

Burton, R. T., Schoenau, G. J., Chan, R. J., 1980, "A Single Stage Precision Flow Divider Valve," *Proceedings of the 36th National Conference on Fluid Power*, Oct., Cleveland, Ohio.

Chan, R. K., Schoenau, G. J., and Burton, R. T., "A Simple Design Modification for Improved Accuracy of Piston Type Flow Divider Valves," *Proceedings of the 35th National Conference on Fluid Power*, Oct., Chicago.

Fedoroff, M., Schoenau, G. J., and Burton, R. T., 1981, "Steady State Characteristics of an Auto-Regulator Valve," *Proceedings of 44th National Conference on Fluid Power*, Cleveland, 1990.

Fedoroff, M., 1990, "Analysis of Steady State and Dynamic Characteristics of an Auto-regulator Valve," M.Sc. Thesis, University of Saskatchewan, Saskatoon, Sask., Canada.

Guo, Q., Burton, R. T., and Schoenau, G. J., 1988, "Dynamic Response of Flow Divider Valves," *Journal of Fluid Control, Including Fluidics Quarterly*, Vol. 19, No. 1, pp. 20-42.

Kwan, D. S., Schoenau, G. J., Burton, R. T., and Wilson, J. N., 1979, "A New High Precision Flow Divider Valve," *Proceedings of the 35th National Conference on Fluid Power*, Chicago, Il., Nov., pp. 61-64.

Simulation Package from Twente University of Technology, IBM PC.
Tauger, M. B., 1972, "Increasing the Precision of Fluid Flow Divider Valves," *Russian Engineering Journal*, Vol. 52, No. 10, pp. 44-46.
Thoma, J. U., 1990, *Simulation by Bondgraphs*, Springer-Verlag, Berlin.
Zhang, Y., and Xin, S., 1989, "Dynamic Analysis of a New Synchronous Valve," *Proceedings of the 1989 International Conference on Fluid Power Transmission and Control*, Hangzhou, PRC, March.
Zhang, Y., Burton, R. T., and Schoenau, G. J., 1984, "Design of a High Precision Flow Divider/Combiner Valve," *Proceedings of 39th National Conference on Fluid Power*, Chicago, Dec.
Zhang, Y. Q., Burton, R. T., and Schoenau, G. J., 1986, "A New Auto-regulated Flow Divider Valve," *Proceedings of 41st National Conference on Fluid Power*, Detroit, April.
Zhang, Y. Q., Burton, R. T., and Schoenau, G. J., 1985, "Some Flow Divider/Combiner Valve Design Considerations," *Proceedings of the 1985 International Conference on Fluid Power Transmission and Control*, Hangzhou, PRC, Sept.
Zhang, Y., Burton, R. T., and Schoenau, G. J., 1988, "An Auto-regulated Flow Divider/Combiner Valve," *Proceedings of 43rd National Conference on Fluid Power*, Chicago.

APPENDIX A

In this appendix the basic describing equations for the linearized model of the auto-regulator are presented. The assumptions for the development of the model were specified in the main body.

$$Q_{D1} = Q_{X1} \tag{A1}$$

$$Q_1 = Q_{D1} + Q_{C1} - Q_C \tag{A2}$$

$$Q_{X1} = A_1 \dot{x}_1 \tag{A3}$$

$$Q_1 = 1/R_{T1}\sqrt{P_{C1} - P_T} \tag{A4}$$

$$Q_{D1} = \frac{P_{X1} - P_{C1}}{R_{D1}} \tag{A5}$$

$$Q_{C1} = Cdw(x_0 + x_1)\sqrt{2(P_S - P_{C1})/\rho} \tag{A6}$$

$$Q_C = C_1 \dot{P}_{L1} \tag{A7}$$

$$m_1 \ddot{x}_1 + b_1 \dot{x}_1 + (k_e x_1) = A_{P1}(P_S - P_{X1}) - F_0 \tag{A8}$$

$$k_e x_1 = 0.43 w x_1 (P_S - P_{C1}) + K_s x_1 \tag{A9}$$

$$P_{SC1} = P_S - P_{C1} \tag{A10}$$

APPENDIX B

In this Appendix, the transfer function relating the pressure drop across the variable orifice to changes in the supply pressure for the auto-regulator is developed. Nonlinearities are linearized by assuming small variations about an operating point. Taking Laplace Transforms and linearizing appropriate equations yields:

$$\Delta Q_{D1} = \Delta Q_{x1} \tag{B1}$$

$$\Delta Q_1 = \Delta Q_{D1} + \Delta Q_{C1} - \Delta Q_C \tag{B2}$$

$$\Delta Q_{X1} = A_1 s \Delta X_1 \tag{B3}$$

$$\Delta Q_1 = f_1 \Delta P_{C1} - f_1 \Delta P_T \tag{B4}$$

$$\Delta Q_{D1} = \frac{\Delta P_{X1} - \Delta P_{C1}}{R_{D1}} \tag{B5}$$

$$\Delta Q_{C1} = f_2 \Delta X_1 + f_3 \Delta P_S - f_3 \Delta P_{C1} \tag{B6}$$

$$\Delta Q_C = C_1 s \Delta P_{C1} \tag{B7}$$

$$m_1 s^2 \Delta X_1 + b_1 s \Delta X_1 + \Delta(k_e x_1) = A_1(\Delta P_S - \Delta P_{X1}) \tag{B8}$$

$$\Delta(k_e x_1) = f_4 \Delta X_1 + f_5 \Delta P_S - f_5 \Delta P_{C1} \tag{B9}$$

$$\Delta P_{(SC1)} = \Delta P_S - \Delta P_{C1} \tag{B10}$$

where:

$$f_1 = \frac{\partial Q_1}{\partial P_1}\bigg|_o = \frac{-\partial Q_1}{\partial P_T}\bigg|_o = \frac{Q_1}{2(P_{C1} - P_T)}\bigg|_o \tag{B11}$$

$$f_2 = \frac{\partial Q_{C1}}{\partial x_1}\bigg|_o = C_d w \sqrt{2(P_S - P_{C1})/\rho}\,|_o \tag{B12}$$

$$f_3 = \frac{\partial Q_{C1}}{\partial P_S}\bigg|_o = \frac{-\partial Q_{C1}}{\partial P_{C1}}\bigg|_o = \frac{Q_{C1}}{2(P_S - P_{C1})}\bigg|_o \tag{B13}$$

$$f_4 = \frac{\partial(k_e x_1)}{\partial x_1}\bigg|_o = [0.43 w(P_S - P_{C1}) + K_S]_o \tag{B14}$$

$$f_5 = \frac{\partial(k_e x_1)}{\partial P_S}\bigg|_o = \frac{-\partial(k_e x_1)}{\partial P_{C1}}\bigg|_o = 0.43 w x_1|_o \tag{B15}$$

Substituting Eqs. (B1), (B3), (B4), (B6), and (B7) into Eq. (B12) and solving for ΔP_{C1} yields:

$$\Delta P_{C1} = \frac{(f_2 + A_{P1}s)\Delta X_1 + f_3(\Delta P_S - \Delta P_{C1})}{f_1 + C_1 s} + \frac{f_1 \Delta P_T}{f_1 + C_1 s} \tag{B16}$$

To solve Eq. (B16) for the desired transfer function, a relationship between the output ΔP_{SC} and ΔP_{X1} was found. Substituting Eq. (B9) into (B8) and (B3) into (B5) yields

$$m_1 s^2 \Delta X_1 + b_1 s \Delta X_1 + f_4 \Delta X_1 + f_5 \Delta P_S - f_5 \Delta P_{C1} = A_{P1}(\Delta P_S - \Delta P_{X1}) \tag{B17}$$

$$\Delta P_{X1} = \Delta P_{C1} + A_{P1} R_{D1} s \Delta X_1 \tag{B18}$$

Substituting Eq. (B18) into (B17) and rearranging yields

$$\frac{\Delta X_1}{\Delta P_{SC1}} = \frac{A_{P1} - f_5}{m_1 s^2 \Delta X_1 + (b_1 + A_{P1}^2 R_{D1})s + f_4} = \frac{K_x \omega_{nx}^2}{s^2 + 2\zeta_x \omega_{nx} s + \omega_{nx}^2} \tag{B19}$$

where $K_x = \dfrac{A_{P1} - f_5}{f_4}$,

$\omega_{nx}^2 = \dfrac{f_4}{m_1}$,

and $\zeta_x = \dfrac{b_1 + A_{P1}^2 R_{D1}}{2\sqrt{m_1 f_4}}$.

Using Eqs. (B16) and (B19), the desired transfer function is obtained.

$$\frac{\Delta P_{SC1}}{\Delta P_s} = \frac{1}{1 + \dfrac{f_3/C_1\{s^2 + [2\zeta_x\omega_{nx} + (A_{P1}K_x\omega_{nx}/f_3)]s + \omega_{nx}^2 + K_x\omega_{nx}^2(f_2/f_3)\}}{(f_1/C_1 + s)(s^2 + 2\zeta_x\omega_{nx}s + \omega_{nx}^2)}} \tag{B20}$$

APPENDIX C

In this appendix, the equations derived from the Bond graph of Fig. 9 are listed. The equations for the divider mode are given only. The equations for the combiner mode are very similar and can be obtained from Fedoroff (1990).

0-Junctions

$$\Delta Q_{SC} = Q_S - Q_{SC}$$

$$Q_{SC} = Q_{C1} + Q_{C2} + Q_{X1} - Q_{X2} + Q_{P1} + Q_{P2}$$

$$\Delta Q_{C1} = Q_{C1} - Q_1 + Q_{D1}$$

$$\Delta Q_{C2} = Q_{C2} - Q_2 - Q_{D2}$$

$$Q_{D1} = Q_{X1} + Q_{P1}$$

$$Q_{D2} = Q_{X2} - Q_{P2}$$

1-Junctions

$$P_{SC} = P_S - \Delta P_E$$

$$\Delta P_{P1} = P_{SC} - P_{X1}$$

$$\Delta P_{P2} = P_{SC} - P_{X2}$$

$\Delta P_{D1} = P_{X1} - P_{C1}$

$\Delta P_{D2} = P_{C2} - P_{X2}$

$\Delta P_{T1} = P_{C1} - P_T$

$\Delta P_{T2} = P_{C2} - P_T$

$F_{M1} = F_{S1} - F_{X1} - F_{F1} - F_{SP} + F_{IMP} - F_{ST1}$

$F_{M2} = F_{X2} - F_{S2} - F_{F2} - F_{IMP} + F_{ST2}$

$\Delta P_{C1} = P_S - P_{C1}$

$\Delta P_{C2} = P_S - P_{C2}$

Transformations

$F_{S1} = P_S A_{P1}$

$F_{S2} = P_S A_{P2}$

$F_{X1} = P_{X1} A_{P1}$

$F_{X2} = P_{X2} A_{P2}$

$Q_{X1} = \dot{x}_1 A_{P1}$

$Q_{X2} = \dot{x}_2 A_{P2}$

R-Effects

R_e: $\Delta P_E = f(Q_{SC})$ Lookup Table

R_{P1}: $Q_{P1} = \Delta P_{P1} / R_{P1}$

R_{P2}: $Q_{P2} = \Delta P_{P2} / R_{P2}$

R_1: $Q_{C1} = Cdw(x_0 + x_1) SGN(\Delta P_1) \sqrt{2ABS(\Delta P_1)/\rho}$

R_2: $Q_{C2} = Cdw(x_0 + x_1) SGN(\Delta P_2) \sqrt{2ABS(\Delta P_2)/\rho}$

R_{T1}: $Q_1 = SGN(\Delta P_{T1}) / R_{T1} \sqrt{ABS(\Delta P_{T1})}$

R_{T2}: $Q_2 = SGN(\Delta P_{T2}) / R_{T2} \sqrt{ABS(\Delta P_{T2})}$

R_{F1}: $F_{F1} = b_1 \dot{x}_1$

R_{F2}: $F_{F2} = b_2 \dot{x}_2$

R_{IMP}: $F_{IMP} = 0$ if $(x_1 - x_2) \geq 0$

$= K_1 (x_1 - x_2)$ if $(x_1 - x_2) < 0$

R_{ST1}: $F_{ST1} = 0$ if $x_1 \leq 0.00125$ m

$= K_{ST1} x_1$ if $x_1 > 0.00125$ m

R_{ST2}: $F_{ST2} =$ if $x_2 \geq 0$ m

$= K_{ST2} ABS(x_2)$ if $x_2 < 0$ m

R_{SP}: $F_{SP} = K_S (x_{S0} + x_1)$

R_{D1}: $\Delta P_{D1} = f(Q_{D1})$ Lookup Table

R_{D2}: $\Delta P_{D2} = f(Q_{D2})$ Lookup Table

I-Effects

I_1: $\dot{x}_1 = 1/I_1 \int F_{M1} dt + \dot{x}_1(0)$

I_2: $\dot{x}_2 = 1/I_2 \int F_{M2} dt + \dot{x}_2(0)$

C-Effects

C_S: $P_S = 1/C_S \int \Delta Q_S dt + P_S(0)$

C_{C1}: $P_{C1} = 1/C_{C1} \int \Delta Q_{C1} dt + P_{C1}(0)$

C_{C2}: $P_{C2} = 1/C_{C2} \int \Delta Q_{C2} dt + P_{C2}(0)$

State Equations

$x_1 = \int \dot{x}_1 dt + x_1(0)$

$x_2 = \int \dot{x}_2 dt + x_2(0)$